Biosensors and Bioelectronics 26 (2011) 2368–2375

Contents lists available at ScienceDirect

Biosensors and Bioelectronics

journal homepage: www.elsevier.com/locate/bios

Enlarged gold-tipped silicon microprobe arrays and signal compensation for multi-site electroretinogram recordings in the isolated carp retina

Tetsuhiro Harimoto[a], Kuniharu Takei[a], Takeshi Kawano[a,*], Akito Ishihara[b], Takahiro Kawashima[c], Hidekazu Kaneko[d], Makoto Ishida[a], Shiro Usui[a,e]

[a] Department of Electronic and Information Engineering, Toyohashi University of Technology, 1-1 Hibarigaoka, Tempaku-cho, Toyohashi, Aichi 441-8580, Japan
[b] School of Information Science and Technology, Chukyo University, 101 Tokodachi, Kaizu-cho, Toyota, Aichi 470-0393, Japan
[c] Department of Mechanical Engineering, Toyohashi University of Technology, 1-1 Hibarigaoka, Tempaku-cho, Toyohashi, Aichi 441-8580, Japan
[d] National Institute of Advanced Industrial Science and Technology (AIST), AIST Tsukuba Central 6, Higashi, Tsukuba, Ibaraki 305-8566, Japan
[e] Laboratory for Neuroinformatics, RIKEN Brain Science Institute, 2-1 Hirosawa, Wako, Saitama 351-0198, Japan

ARTICLE INFO

Article history:
Received 24 July 2010
Received in revised form
29 September 2010
Accepted 11 October 2010
Available online 16 October 2010

Keywords:
Multi-electrode array (MEA)
Vapor–liquid–solid (VLS) growth method
Silicon microprobe array
Electroretinogram (ERG)
Parasitic capacitance
Signal compensation

ABSTRACT

In order to record multi-site electroretinogram (ERG) responses in isolated carp retinae, we utilized three-dimensional (3D), extracellular, 3.5-μm-diameter silicon (Si) probe arrays fabricated by the selective vapor–liquid–solid (VLS) growth method. Neural recordings with the Si microprobe exhibit low signal-to-noise (S/N) ratios of recorded responses due to the high-electrical-impedance characteristics of the small recording area at the probe tip. To increase the S/N ratio, we designed and fabricated enlarged gold (Au) tipped Si microprobes (10-μm-diameter Au tip and 3.5-μm-diameter probe body). In addition, we demonstrated that the signal attenuation and phase delay of ERG responses recorded via the Si probe can be compensated by the inverse filtering method. We conclude that the reduction of probe impedance and the compensation of recorded signals are useful approaches to obtain distortion-free recording of neural signals with high-impedance microelectrodes.

1. Introduction

Multi-channel recordings of retinal responses, arising from photoreceptors, to retinal ganglion cells (output neurons of the retina) are useful for analyzing spike-coding mechanisms of the retina. Almost all retinal neurons generate graded potentials, but ganglion cells and some amacrine cells generate spike potentials (Rodieck, 1973). For multi-channel recordings of the retinal spike potential, multi-electrode array (MEA) is an effective tool. In previous papers, planar MEAs and silicon (Si)-based MEAs have been used for the study of the relationship between a light stimulus and spike pattern of the retinal ganglion cells (Meister et al., 1994; Greschner et al., 2002; Olveczky et al., 2003; Ishikane et al., 2005).

Multi-electrode arrays (MEAs) have not been used for multi-channel recordings of retinal neurons other than retinal ganglion cells (e.g., bipolar cell, horizontal cell and amacrine cell). The multi-channel recordings of various retinal neurons, before conversion into spike potentials, are also important for analyzing the spike-coding mechanisms. The summed response of various retinal neurons to a brief white flash stimulus can be recorded as a flash electroretinogram (ERG), which exhibits a negative-going response (a-wave), followed by a slower positive component (b-wave). The ERG a-wave originates from photoreceptors (Penn and Hagins, 1969), and the ERG b-wave is mainly contributed by the activity of bipolar cells (retinal secondary neurons) (Sieving et al., 1994). The recording of these multi-site ERG a- and b-waves could be powerful for further investigation of functional mechanisms of the retina, because spatial distribution is an important characteristic in studies on the retina (Wilms and Eckhorn, 2005). However, the conventional method of ERG recording was to use a pair of glass (or metal) electrodes. In order to obtain a spatial distribution of ERG responses, the use of focal light stimuli to the retina, for example a small spot under background light (Miyake, 1998), and a multifocal flicker stimulus have been proposed (Sutter and Tran, 1992). If MEAs are applied to the ERG recording, on the other hand, the spatial distribution of ERG responses would be obtained without restricting the pattern of the light stimulation, and the recoding of higher spatial resolution of ERG responses would be possible.

In order to directly record multi-site ERG responses, we have developed an Si microprobe array-based MEA fabricated by the selective vapor–liquid–solid (VLS) growth method (Kawano et al., 2003, 2010). The penetrating MEA is suitable for the isolated retina

* Corresponding author. Tel.: +81 532 44 6738; fax: +81 532 44 6738.
E-mail address: kawano@ee.tut.ac.jp (T. Kawano).

0956-5663/$ – see front matter © 2010 Elsevier B.V. All rights reserved.
doi:10.1016/j.bios.2010.10.014

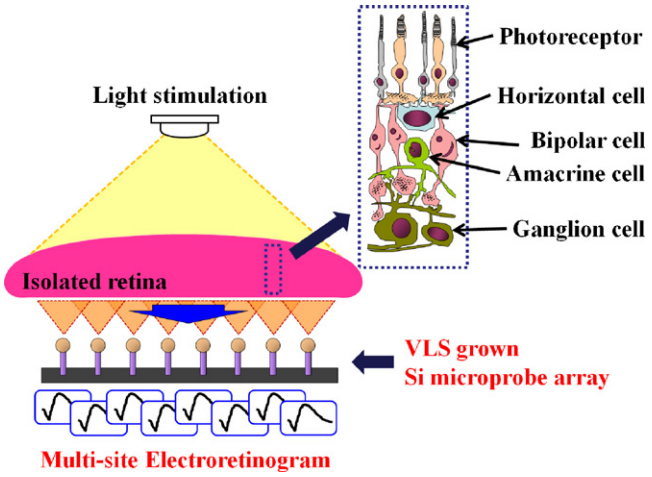

Fig. 1. Multi-site electroretinogram (ERG) via vapor–liquid–solid (VLS) grown silicon (Si) microprobe array.

because the electrode, through the residue of the vitreous, results in good electrical contacts with the retina (Segev et al., 2007). The shape of the Si microprobe array is similar to Utah's MEA (Jones et al., 1992), but the VLS growth-based Si microprobes allow fabricating smaller diameters (<4 μm), and there are higher densities (<100 μm) of electrodes than Utah's MEA. Because of the small diameters of the probe bodies and probe tips, the Si microprobes promise an additional advantage of minimal damage to retinal tissue/neurons during electrode penetration. The Si microprobe array also allows on-chip microelectronic configurations for additional neuroscience applications (Kawano et al., 2004).

We have previously characterized the use of the Si microprobe in extracellular electrical neural recordings and demonstrated recordings of ERG responses with isolated carp retinae (Kawano et al., 2010). Although we demonstrated the neural recording from the retina using two-channel Si microprobes, there are technological issues to be addressed for further multi-site ERG recordings; for example, for small retinal signals of ERG waves (amplitude of less than 100 μV): (1) fabricated sub-4-μm-diameter probes exhibit high-impedance characteristics due to the small effective recording area, (2) impedance variation of the probe is observed and the process of reducing/adjusting impedance of the probe is necessary, and (3) the signal attenuation and phase delay by parasitic capacitances cannot be ignored in the use of high-impedance electrodes.

Here we discuss the use of enlarged gold (Au) tipped Si microprobe arrays and a signal compensation method for multi-site ERG recordings (Fig. 1). The Au electroplating to the probe tip reduces the probe impedance due to the enlarged effective recording area at the probe-tip section without increasing the diameter of the probe body. Based on the investigation of the electrical properties of the Si microprobe chip and recording system, the signal-attenuated and phase-delayed recorded ERG responses were compensated. We then demonstrated an 8-channel ERG recording by utilizing both proposed methods of the enlarged Au-tipped Si microprobe array and signal compensation of recorded ERG responses.

2. Methods

2.1. Enlarged Au-tipped Si microprobe arrays

A 3 × 10 Si microprobe array was designed with 100 μm electrode-spacing, as shown in Fig. 2a. The fabrication process of the Si microprobe array was similar to the procedure used in our previous study (Takei et al., 2008). The Si microprobes with a length of 40 μm and a diameter of 3.5 μm were fabricated on an Si substrate. The Si microprobes were integrated with IC-processed interconnections of multiple layers of metals [300-nm-thick tungsten silicide (WSi_2)/50-nm-thick titanium nitride (TiN)/50-nm-thick titanium (Ti); the gap between interconnections is 50 μm]. The length and width of each interconnection are 3.5 mm and 10 μm, respectively. The thickness of the silicon-dioxide (SiO_2) insulating layer between the interconnection and the substrate is 1.8 μm. The sidewall of the Si microprobes were covered with a 500-nm-thick SiO_2 insulating layer formed by plasma-enhanced chemical vapor deposition (PECVD) followed by etching the deposited SiO_2 from the probe tips using the etch-back technique. A black resist layer (optical density = 3.0 at 1 μm thickness; resistivity is 10^{14} Ω/sheet) was spun on the surface of the device except for the probe tips in order to shield the chip against the light stimulation used in the neural recordings.

To decrease the electrical impedance of the probe in saline, we used an Au-electroplating method to make the enlarged 10-μm-diameter Au-tipped Si microprobe. First, the electrode chip was dipped into an electrolyte solution (MicroFab Au620) (solution temperature = 60 °C); each microprobe to be plated was connected with a cable as the cathode. Second, a nickel electroplated plate was immersed in the electrolyte solution, as the anode. By applying a constant bias of 500 mV between the anode and the cathode, we can control Au thickness with deposition time. We found that 25 s electroplating results in an enlarged microprobe tip from 3.5 μm to 10 μm in diameter. Fig. 2b shows the scanning electron microscope (SEM) image of the enlarged Au-tipped Si microprobe. All of the probe-bodies had a constant diameter of 3.5 μm, as shown in Fig. 2b and c. The parameters of the electroplating are bias = 500 mV (DC), plating-time = 25 s, and a solution temperature = 60 °C.

For the *in vitro* retinal recording, we used a recording chamber consisting of a Petri dish, which was glued onto the ceramic package and sealed with silicone to ensure a watertight connection (Fig. 2d and e). During the neural recording, a silver/silver chloride (Ag–AgCl) coated wire was used as a reference electrode and was formed as a loop which to line the inside of the chamber. We used eight probes in the array for all of the neural recordings in this study (Fig. 2a), because the other 22 probes were broken or high impedance probes (>5 MΩ at 500 Hz). To obtain a higher fabrication yield of the probe array, the process parameters in the microfabrication steps as well as the selective VLS growth step could be improved.

2.2. Embedded parasitic impedance model

An equivalent circuit model of the Si microprobe array chip is depicted in Fig. 3a and b. The impedance Z_{para1} consists of parasitic capacitances existing at the probe side (C_{side} = 0.03 pF, see Appendix A) and between the metal and saline ($C_{metal/saline}$ = 0.46 pF, see Appendix A):

$$Z_{para1}(j\omega) = \frac{1}{j\omega(C_{side} + C_{metal/saline})} \quad (1)$$

The impedance Z_{para2} consists of parasitic capacitances and a parasitic resistance between the signal line and the ground. These parasitic capacitances exist at the p–n junction (C_{p-n} = 0.9 pF, see Appendix A), between the metal interconnection and the substrate ($C_{metal/substrate}$ = 0.1 pF, see Appendix A), and between the signal line and the reference line from the Si microprobe chip to the pre-amplifiers (C_{cable} = 130 pF, measured value). Due to the p–n junction in between the metal interconnection and microprobe, a parasitic resistance (R_{para} = 7 MΩ representative measured value), which was confirmed experimentally, should be considered in the

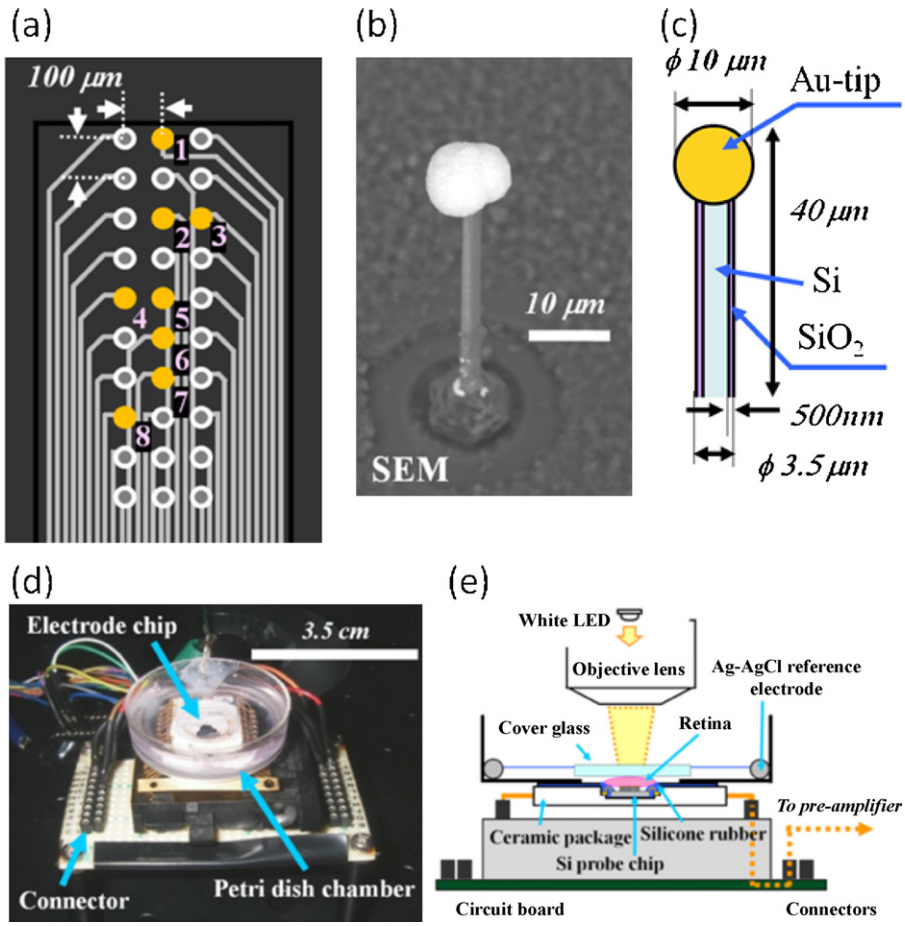

Fig. 2. The enlarged Au-tipped Si microprobe array and the recording chamber. (a) Electrode layout for a 3 × 10 array with 100 μm spacing. The eight probes used in this study are marked in yellow. Broken probes or probes with high impedance were excluded from the measurements. The numbers here correspond to the numbers in Fig. 5. (b) A scanning electron microscope (SEM) image and (c) a schematic cross-section of the Si microprobe are shown. Each probe's body was 40 μm in length and 3.5 μm in diameter. The probe head of the Si microprobe is Au and 10 μm in diameter. (d) Photograph and (e) schematic diagram of a Si microprobe chip packaged with the chamber. The isolated retina of a carp fish is placed over the chip in the recording chamber filled with Ringer's solution. LED light stimuli were irradiated through the microscope tube onto the retina. (For interpretation of the references to color in this figure legend, the reader is referred to the web version of the article.)

equivalent circuit model as a parallel current path:

$$Z_{para2}(j\omega) = \frac{R_{para}}{1 + j\omega(C_{metal/substrate} + C_{p-n} + C_{cable})R_{para}} \quad (2)$$

The coupling capacitance between neighboring interconnections might cause crosstalk via integrated interconnections in the Si microprobe chip (C_{metal} = 0.8 pF, calculated value), interconnections from ceramic package section to the circuit board section (C_{pack} = 3 pF, measured value), and signal lines of the cable bundle from the circuit board to pre-amplifier section (10×, Alpha MED Scientific, Japan) (C_{line} = 30 pF, measured value). We neglected the crosstalk capacitances between adjacent interconnections because currents do not flow through the coupling capacitances. This condition is caused when the entire retina is stimulated by uniform light, and similar evoked retinal signals are simultaneously recorded at all recording channels via Si microprobes (see Appendix B). Additionally, electrical resistances associated with the aforementioned interconnections are neglected for the calculation, because these resistances (1.2 kΩ) are significantly smaller than the aforementioned parasitic impedances (see Appendix A).

2.3. The cell–electrode interface model

Fig. 3c and d describe equivalent circuit models of an individual Si microprobe for (1) a test signal recording without placing cells over the probe tip (Fig. 3c), and (2) a neural recording with a retina over the surface of the probe tip (Fig. 3d). During the test signal recording with an Ag–AgCl electrode (Fig. 3c), Z_{para1} is electrically connected in parallel to probe impedance Z_p, because Z_{para1} is electrically connected with the stimulating electrode (i.e., input signal, V_{Ein}) via saline. The output signal V_{Eout} was recorded through the Si microprobe chip. The recorded V_{Ein} is the same as the input signal, because the impedance of the Ag–AgCl electrode is negligibly small (1 kΩ at 1 kHz) (Dendo, 2000). The transfer function in a test signal recording H_E is expressed in the following equation:

$$H_E(j\omega) = \frac{V_{Eout}(j\omega)}{V_{Ein}(j\omega)} = \frac{Z_{load}//Z_{para2}}{Z_p//Z_{para1} + Z_{load}//Z_{para2}} \quad (3)$$

where Z_{load} is the load impedance and $Z_{load} = R_{amp}/(1 + j\omega R_{amp}C_{amp})$. R_{amp} and C_{amp} represent the input resistance (R_{amp} = 10 GΩ) and the input capacitance (C_{amp} = 2 pF) of the pre-amplifier.

During the neural recording, as a retina covers the surface of the Si microprobe (Fig. 3d), Z_{para1} is grounded through the additional reference electrode (Ag–AgCl) via solution. The input signal V_{Nin} is a cell–electrode interface voltage, which is close to the probe tip, and the output signal V_{Nout} is observed as neural signals. Thus, the transfer function in a neural recording H_N is described with the

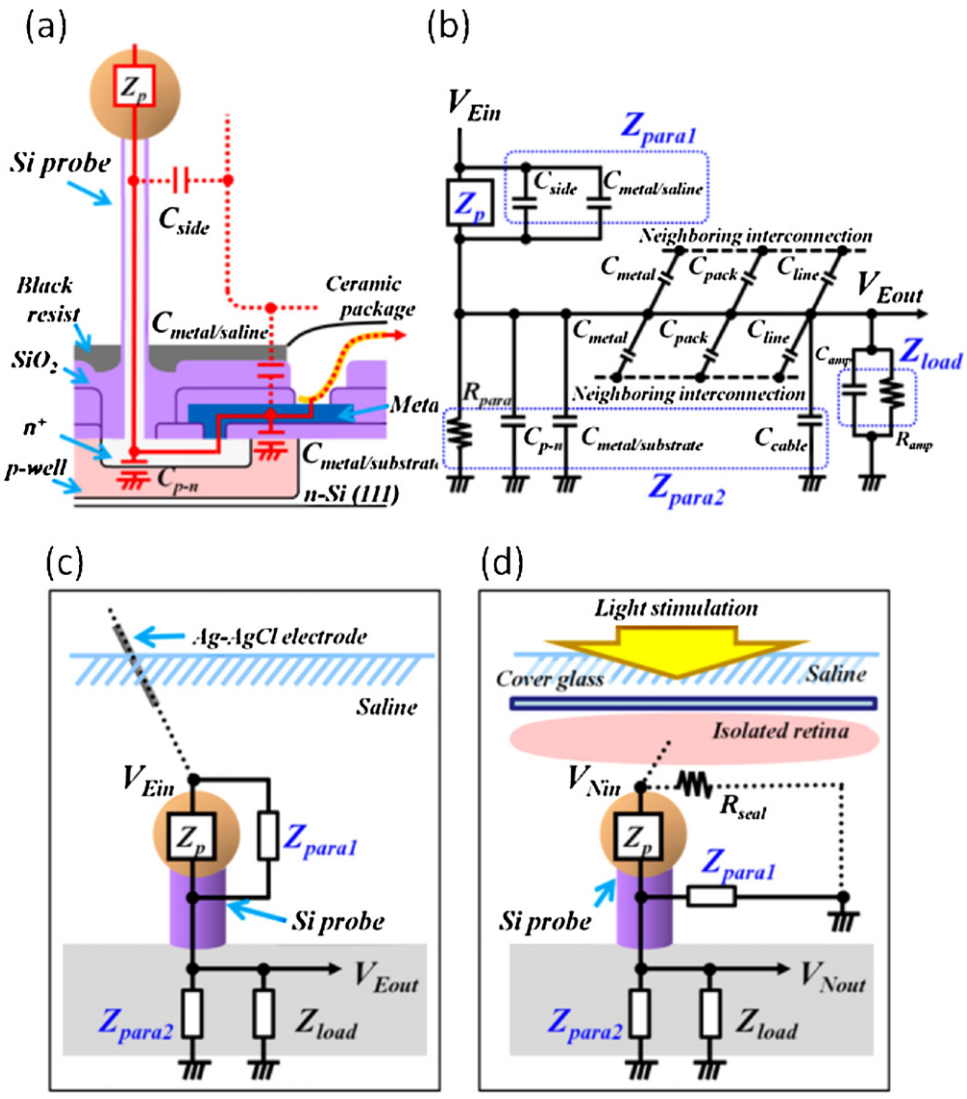

Fig. 3. The equivalent circuit of the Si microprobe during the test signal recording and the neural recordings. (a) Parasitic capacitance model of Si microprobe chip. Parasitic capacitances exist at the probe side (C_{side}); between the metal and saline solution ($C_{metal/saline}$); the p–n junction (C_{p-n}); between the metal interconnection and the substrate ($C_{metal/substrate}$); and between the signal lines and a reference line of cables (C_{cable}) (array chip – first amplification). C_{cable} and C_{amp} are not shown in (a). (b) A detailed model of the recording system during electrical stimulation and recordings. (c) A simplified model of the recording system during the electrical stimulation and recordings. Z_{para1} is electrically connected in parallel to probe impedance Z_p, since the C_{side} and $C_{metal/saline}$ are electrically connected with the source (input signals) via solution. Z_{load} is the input impedance of the pre-amplifier [$R_{amp}//1/(j\omega C_{amp})$]. (d) A simplified model of the recording system during neural recordings.

following equation:

$$H_N(j\omega) = \frac{V_{Nout}(j\omega)}{V_{Nin}(j\omega)} = \frac{Z_{load}//Z_{para1}//Z_{para2}}{Z_p + Z_{load}//Z_{para1}//Z_{para2}} = \frac{|V_{Nout}(j\omega)|}{|V_{Nin}(j\omega)|}\{\cos(\theta_N) + j\sin(\theta_N)\} \quad (4)$$

where θ_N is the phase delay of H_N, as observed by a phase difference between the input signal V_{Nin} and the output signal V_{Nout}. We considered that H_N is the minimum phase system, because the $|H_N|$ in this study was not zero at any frequency less than the sampling frequency.

2.4. Probe impedance derivation

During the test signal recording, the output/input signal ratios (O/I ratio), which is an absolute value of the transfer function $|H_E|$, are experimentally given by the observed V_{Eout} and V_{Ein}. The phase delay θ_E of H_E is also given by a phase difference between the input signal and the output signal. Therefore, H_E can be described as

$$H_E(j\omega) = \frac{|V_{Eout}(j\omega)|}{|V_{Ein}(j\omega)|}\{\cos(\theta_E) + j\sin(\theta_E)\} \quad (5)$$

Using Eqs. (3) and (5), the probe impedance Z_p can be estimated as follows:

$$Z_p(j\omega) = \frac{Z_{para1}(Z_{load}//Z_{para2})(1 - H_E)}{H_E(Z_{para1} + Z_{load}//Z_{para2}) - Z_{load}//Z_{para2}} \quad (6)$$

2.5. Amplitude- and phase-compensation

In order to estimate $V_{Nin}(t)$, the amplitude- and phase-compensation of $V_{Nout}(t)$ are conducted using an inverse filtering method. During the test signal recordings (Fig. 3c), V_{Ein} and V_{Eout} are given by the stimulated input sine signals and the recorded output signals, respectively. In the neural recording (Fig. 3d), the unknown V_{Nin} is given as observed responses V_{Nout}:

$$V_{Nout}(j\omega) = H_N(j\omega) \cdot V_{Nin}(j\omega) \Rightarrow V_{Nin}(j\omega) = H_N^{-1}(j\omega) \cdot V_{Nout}(j\omega) \quad (7)$$

where H_N can be calculated by Eq. (4), in which the probe impedance Z_p is estimated by Eq. (6). Specifically, we used the Fourier transformation on the raw data, and the compensation was done at every frequency less than 500 Hz. To convert the compensated signal into the time domain, the inverse Fourier transformation was used. Since the $|H_N|$ in this study was not zero at any frequency less than the sampling frequency, H_N is considered to be minimum phase system. Because attenuated and phase-delayed neural responses caused by parasitic capacitances (Fig. 3b) were obtained, H_N can be approximated by a low-pass filter. Thus, we approximated the amplitude and the phase characteristics of H_N by appropriate sigmoid functions and then expressed the inverse filter as follows (see Appendix C):

$$H_N^{-1} = G_{amp}\left\{\cos(\theta_c) + j\sin(\theta_c)\right\} \tag{8}$$

$$G_{amp} = \left|H_N\right|^{-1} = \left(\frac{1}{1+\alpha\exp\{\beta[\log_{10}(f)+\gamma]\}}\right)^{-1} \tag{9}$$

$$\theta_c = -\arg H_N = \frac{0.436}{1+\eta\exp\{\lambda[\log_{10}(f)+\tau]\}} \tag{10}$$

where G_{amp} and θ_c are the inverse of the approximated O/I ratio ($|H_N|$) and the opposite of the approximated phase delay ($\arg H_N$), respectively. The model parameters (α, β, γ, η, λ and τ) of the O/I ratio ($|H_N|$) and phase delay ($\arg H_N$) are estimated by applying the least-squares-fitting of the sigmoid function. Because electrode impedances and parasitic capacitances of signal lines were considered to be different between probes, we used inverse filters with respect to each probe.

2.6. Preparation of isolated carp retina

Neuronal recordings were carried out with carp (*Cyprinus carpio*, 20–35 cm in length), which were kept in a water tank at room temperature and raised on a 12-h light on/12-h light off cycle. Before the recording, the carp was dark adapted for at least 1 h. All efforts were made to minimize the fish's suffering and to reduce the number of fish used in the experiment based on our institutional animal care guidelines.

The eye of the carp was removed and a small cut was made near its equator using a sharp blade. The eyeball was carefully cut and opened with fine scissors and the cornea and lens were separated from the posterior half. After soaking for a few minutes in hyaluronidase (0.1 mg/10 ml)—containing Ringer's solution (saline for retina), the vitreous were then gently scooped out with a small brush. After all of the vitreous was removed and soaked, the inverted eyecup was put on a filter paper. The retina was peeled with fine tweezers from the edge of the eyecup towards the optic nerve head. The retina was completely separated by cutting the optic nerve. Finally, the isolated retina was transferred into the recording chamber and was mounted with the ganglion cell layer on the Si microprobe array chip. A cover glass (TROPHY Micro Coverglass 18 mm) was placed on the retina to provide weight, and small quantity of the Ringer's solution was poured into the dish chamber (Fig. 2e). All procedures were performed under dim red light. Retinal isolation and test signal recording were performed in Ringer's solution. In our experiment, the Ringer's solution was composed of (in mM): 120 NaCl, 2.6 KCl, 1.0 $MgCl_2$, 1.0 $CaCl_2$, 28.0 $NaHCO_3$, and 5.0 glucose buffer to pH 7.6 (Asano, 1977).

2.7. Electrical and neural recordings

We characterized the frequency-dependent impedance characteristics of the Si microprobe chip in 0.9% NaCl solution using a counter electrode of Ag–AgCl (impedance = 1 kΩ at 1 kHz). The impedance of the Si microprobe chip section (impedance between "Ag–AgCl electrode" and "V_{Eout}" in Fig. 3c) was measured with a frequency response analyzer (FRA) (Model 1260A; Solartron Analytical, UK). In order to obtain the O/I ratio and phase delay of the fabricated Si microprobe chip in saline solution (Ringer's), the electrical recording with test signals was conducted as shown in Fig. 3c. The test signals were generated by a function generator (SG-4105, Iwatsu Electric, Tokyo, Japan). Signals were recorded by a computer (A/D board: 12 bits) through pre-amplifiers (10×), main-amplifiers (1000×), and 0.1 Hz to 10 kHz band-pass filter (MED64 System; Alpha MED Scientific, Osaka, Japan). The amplified and filtered signals were digitized by a 12-bit resolution data acquisition board operating at 20,000 samples/s/electrode. The digitized data were displayed on a monitor screen and stored onto the computer hard disk (Pentium computer, Windows 2000).

In neural recordings, retinal responses were evoked by a white light-emitting diode (LED) stimulus (Luxeon; Philips Lumileds, San Jose, CA). The stimulator was mounted on the camera port of an upright microscope (BX51WI; Olympus, Tokyo, Japan). LED light stimuli were irradiated through the microscope tube onto the retina. The illumination intensity and duration of light stimuli were controlled by a function generator (SG-4105; Iwatsu Electric, Tokyo, Japan). Neural responses were recorded by the same data acquisition system as the electrical test signal recordings.

3. Results

3.1. Enlarged Au-tipped and non-electroplated Si microprobe array

In order to compare non-electroplated Si microprobes with enlarged Au-tipped Si microprobes, the impedance and phase delay were measured. Fig. 4a shows a representative example of an impedance magnitude and phase delay of the Si probe chip section (impedance between "Ag–AgCl electrode" and "V_{Eout}" in Fig. 3c). The measured impedance of the chip with an enlarged Au-tipped Si microprobe was 1.36 MΩ (−48.8°) at 1 kHz. In contrast, the chip with a non-electroplated Au-tipped Si microprobe was measured to have higher impedances (e.g., 7.33 MΩ, –48.3° at 1 kHz). As we used same configuration of the chip and recording system for both probe measurements, except for the difference in the probe-tip section, we confirmed that the impedance reduction was due to the enlarged Au tip formed by the Au electroplating (Fig. 4a, top). However, the phase delay yielded similar values for both probes (Fig. 4a, bottom).

3.2. Output/Input ratios of enlarged Au-tipped Si microprobe array

In order to obtain inverse filters for signal compensation (see Section 2.5), we estimated O/I ratios ($|H_N|$) and phase delays ($\arg H_N$) during the neural recordings; we based these on the O/I ratios ($|H_E|$) and phase delays ($\arg H_E$) measured in the test signal recordings (see Section 2.3) and the estimated probe impedance (see Section 2.4). The O/I ratio and phase delay of the enlarged Au-tipped Si microprobe array were obtained by measuring output signals while peak-to-peak 80 μV sine-wave signals (50 Hz to 1 kHz) were applied into the saline in the chamber (Fig. 3c). Fig. 4b shows measured O/I ratios ($|H_E|$) and phase delays ($\arg H_E$) of each Si microprobe including the recording system during the test signal recording. The averaged O/I ratio and phase delay of the probe chip with the enlarged Au tip obtained from the test signal recording were $47.8 \pm 2.7\%$ and $-17.7 \pm 5.8°$, respectively, at 1 kHz (dashed lines in Fig. 4b).

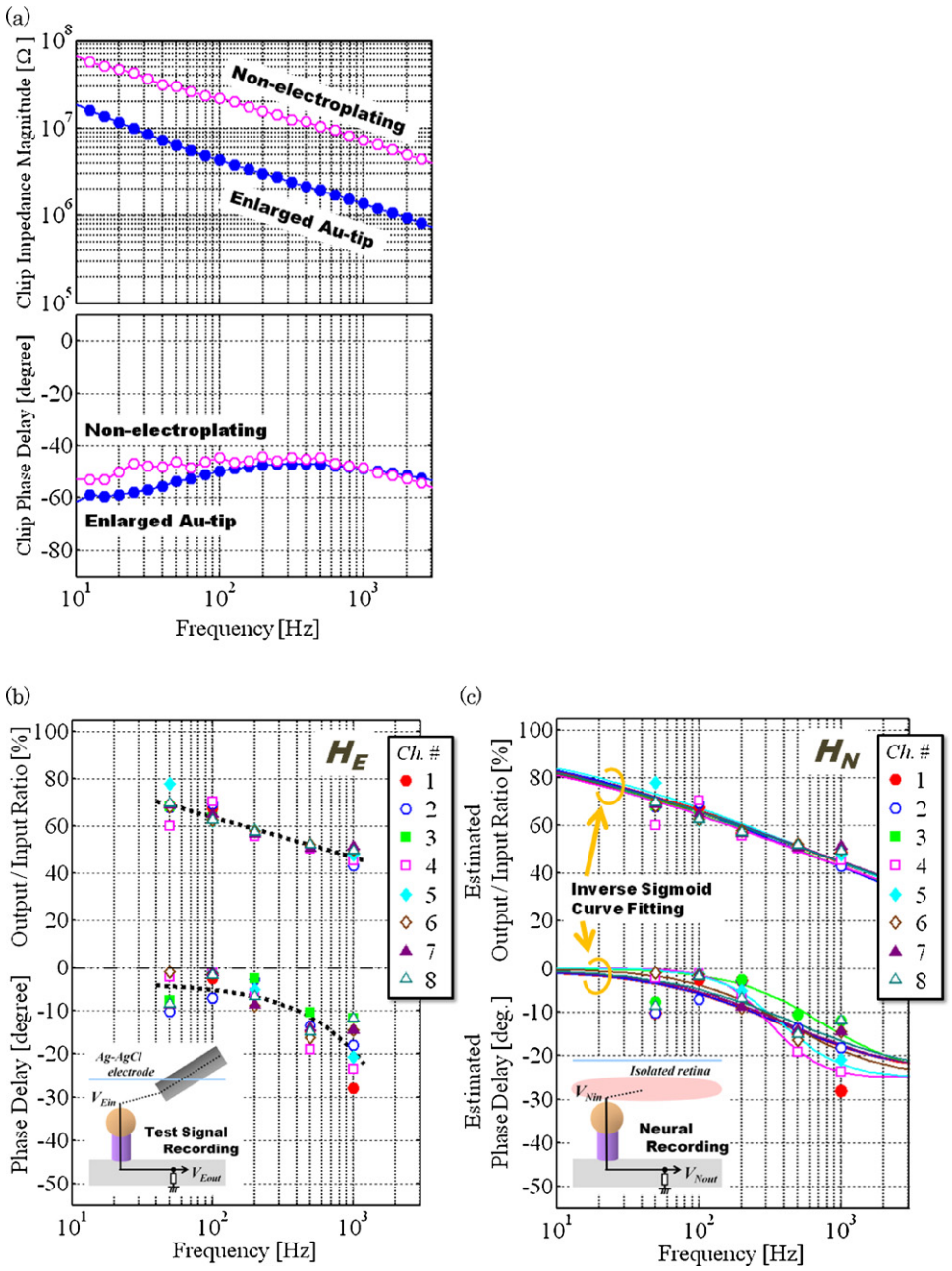

Fig. 4. Electrical properties of the Si microprobe array and the recording system. (a) The impedance magnitude (top) and phase delay (bottom) of the Si probe chip section (impedance between "Ag–AgCl electrode" and "V_{Eout}" in Fig. 3c). (b) The measured O/I ratios and phase delays during the test signal recordings. The signals recorded with the Si microprobe array via Ringer's solution. The input signal with 80 μV_{pp} sinusoid (50 Hz to 1 kHz) was applied using an Ag–AgCl electrode. Both input and output signal are averaged ($n = 100$) and filtered (low pass: 10 kHz). The dashed lines (black) are approximated curves which are fitted to average values by the least squares method. (c) Estimated O/I ratios and phase delays of Si microprobes during neural recording. The data points were obtained from calculated Z_p and Eq. (4). Solid lines are inverse sigmoid curves fitted to each estimated values.

In order to estimate O/I ratios ($|H_N|$) and phase delays ($\arg H_N$), we calculated impedances of the Si microprobes by using Eqs. (5) and (6) (see Section 2.4); this resulted in a probe impedance Z_p of $1.4 \pm 0.2\,M\Omega$ ($-47.7 \pm 9.6^\circ$) at 1 kHz. The data points shown in Fig. 4c were both the estimated O/I ratios ($|H_N|$) and phase delays ($\arg H_N$) given from the calculated Z_p and Eq. (4); and demonstrates that there were no significant differences in the O/I ratio and phase delay between the frequency characteristics of the test signal recordings and neural recordings (Figs. 4b and c). This is due to the negligible contribution of the parasitic impedance Z_{para1} (see Appendix A): In the test signal recording, Z_{para1} is connected to the probe impedance Z_p in parallel (Fig. 3c), and Z_{para1} is grounded in the neural recording (Fig. 3d). The averaged O/I ratio and phase delay at 1 kHz were estimated to be $47.7 \pm 2.7\%$ and $-17.9 \pm 5.9^\circ$, respectively, and we used these estimations for signal compensation of the recorded ERG responses.

3.3. Multi-site ERG recording

In the multi-site ERG recording with Si microprobes, the retina was stimulated with full-field white stimuli, which were 1300 lx and 1 ms duration. Fig. 5a and c (blue lines) show light-evoked ERG responses recorded from Si microprobes in the array. Each blue-lined response was obtained by averaging repetitively recorded

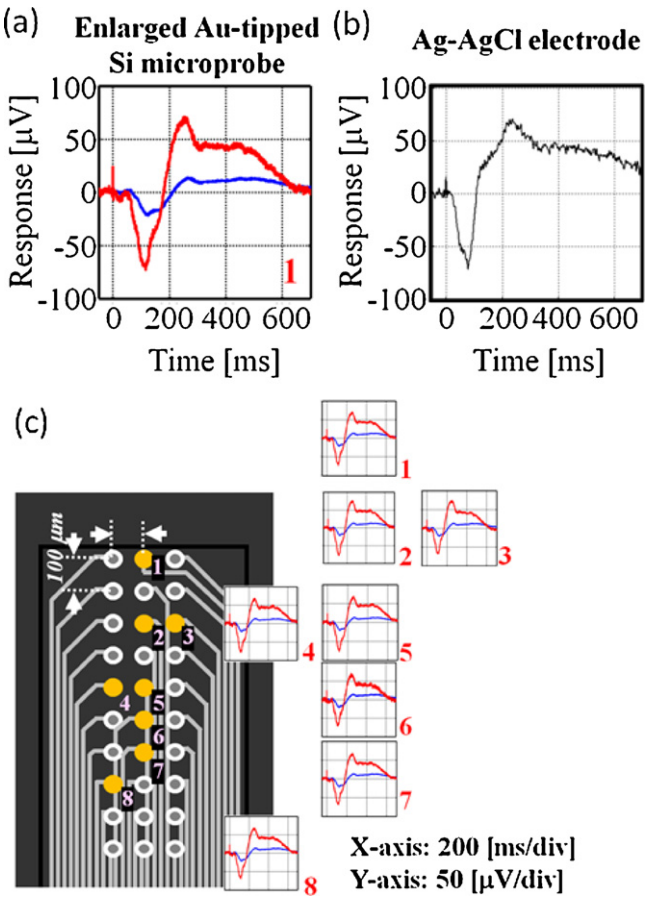

Fig. 5. Multi-site ERG from the carp's isolated retina from the Si whisker microprobe array. (a) ERG responses recorded from channel #1 of the enlarged Au-tipped Si microprobe in the array. The two types of the ERG responses are before (blue) and after (red) amplitude- and phase-compensation. The recorded responses (blue) to a 1 ms flash (1300 lx) were processed with averaging ($n = 5$) and low-pass filtered ($f_c = 500$ Hz). The first transient positive component at the light stimulus was an artifact and not a retinal response (0 ms). (b) A conventional Ag–AgCl electrode detected an ERG response (not simultaneous but separate recording). The signal compensation method was not used for the Ag–AgCl electrode because of the low enough impedance for use in ERG recordings. (c) Multi-channel recording of ERG responses. (For interpretation of the references to color in this figure legend, the reader is referred to the web version of the article.)

ERG responses ($n = 5$) and then filtering the averaged response with a low-pass filter ($f_c = 500$ Hz). The responses were averaged at each sampled data point based on stimulus timing. The transient positive component after the presentation of the light stimulus was an artifact and not a retinal response. The amplitude of the a-wave is defined as the potential difference from the baseline to the negative peak. The amplitude of the b-wave is a difference between the peak of the a-wave and the following positive peak. In addition, the implicit times of the a-wave and b-wave are defined as the time difference between light stimuli and the peak of each wave. The average amplitude and implicit time of the measured ERG a-wave were 19.6 ± 0.43 μV and 125.2 ± 1.2 ms, respectively; while the ERG b-wave measured 29.9 ± 0.65 μV and 265.1 ± 0.9 ms. Fig. 5b is a representative example of the ERG response, which was not simultaneously recorded with an Ag–AgCl electrode (electrode impedance $\ll 1$ MΩ, 1 kHz). Herein, the signal compensation method was not used for the Ag–AgCl electrode because of the low enough impedance for use in ERG recordings. We used two enlarged probe-head electrode array chips for retinal recordings. ERG responses similar to Fig. 5a were also observed using the other chip.

3.4. Amplitude- and phase-compensation

In order to compensate the amplitude and phase of recorded ERG responses, we built inverse filters expressed by sigmoid curves [Eqs. (8)–(10)]. The average of the filter parameters estimated by the least squares curve-fitting were: $\alpha = 0.079 \pm 0.007$, $\beta = 0.9 \pm 0.04$, $\gamma = 0.11 \pm 0.001$, $\eta = 7.88 \pm 0.02$, $\lambda = -3.1 \pm 0.04$, and $\tau = -1.87 \pm 0.25$. The measured ERG responses were compensated by using the aforementioned inverse filters [see Eq. (7)]. Fig. 5a also shows ERG responses after the signal compensation (red line). Similar signal compensations of the recorded ERGs were also conducted for all recorded ERGs, as shown in Fig. 5c. If different responses are obtained via other enlarged probe-head electrode array chips due to differences in the electrical characteristics of the probe, we still can use the signal compensation method for each device to obtain ERG responses by the following: (1) test signal recording to make compensation curve, (2) actual ERG recoding, and (3) signal compensation.

4. Discussion

In order to obtain multi-site ERG responses, we proposed the use of both the enlarged Au-tipped Si microprobe array and the conducted signal compensation based on the embedded parasitic impedance model of the recording system. Here we discuss the relationship between the electrical properties (probe impedance, O/I ratio) and the recording area of the probe tip; and the signal comparison between signal compensated ERGs recorded by the Si microprobe and a typical ERG by a conventional Ag–AgCl electrode. We also discuss further improvements of the recording system which would be required for future retinal recordings.

The enlargement of recording areas by Au-electroplating was an effective way to obtain lager O/I ratios of retinal signals. We had previously investigated the electrical properties of the non-electroplated Si microprobe with the same diameter of 3.5 μm, and the O/I ratio was 21% at 1 kHz in that experimental system (Takei et al., 2010). This is the ratio that was increased by applying the enlarged Au tip in the current study (Fig. 4b and c). The estimation gives the reduction of the probe impedance from 7.3 MΩ (non-electroplated Si probe) to 1.4 MΩ (enlarged Au-tipped Si probe), which corresponds to a decrease factor of 0.2. The recording surface area of the non-electroplated 3.5-μm-diameter Au tip can be approximated to be 19 μm^2 (hemispherical tip shape). Compared to an electroplated enlarged 10-μm-diameter Au tip (spherical-like-tip shape) with a surface area of ~304 μm^2, the electrode surface increased by a factor of 16. The Au electroplating increased the O/I ratio from 21% (non-electroplating, Takei et al., 2010) to 48% (Au electroplating), which is a result of the increase in the recording surface area of the probe (see Fig. 4).

We compensated the attenuated and phase-delayed retinal signals by the electrical properties of the Si microprobe chip and the parasitic capacitances of the recording system, and were able to obtain differentiated negative (a-wave) and positive (b-wave) components of the recorded ERG responses (Figs. 5a and b). Both ERG components can be used for the further evaluation of retinal functions. Even though we were able to record ~35 μV ERG responses from the isolated carp retina because of the enlarged Au-tipped Si microprobe (1.4 MΩ, 1 kHz) (Fig. 5a), both ERG a- and b-waves exhibited smaller amplitudes and distorted waveforms compared to a typical ERG response recorded in another recording session with an Ag–AgCl electrode (Fig. 5b). The waveform distortion was due to the electrical properties of the Si probe chip and embedded parasitic capacitances of the recording system. By compensation of the attenuated and phase-delayed ERG responses with the transfer function (O/I ratio and phase delay) of the Si microprobe chip and the recording system, we obtained increased a- and b-wave

amplitudes, which were similar to the waveform of ERG responses recorded by the Ag–AgCl electrode (Fig. 5a and b): the difference in the recorded responses of the electrodes can be explained by the different recording areas. The recording area of the Si-microprobe and Ag–AgCl electrode were 304 μm^2 and 3 mm^2, respectively. In waveform comparisons of recorded ERGs responses via Si microprobes, we found no significant difference in waveform between the used eight probes, due to the full-field light stimulus and the design of the Si microprobe array; a local light stimulation system, a larger recording area of the probe array (>200 $\mu m \times 700\ \mu m$) as well as an increased number of probes (>8 probes) are required for further discussion on the spatial distribution of the ERG.

Our systematic analysis using the parasitic impedance model allows optimal configurations of both the Si microprobe chip and the recording system. In order to obtain an O/I ratio of more than 90% ($|Z_{load}| = 80\ M\Omega$; $|Z_{para1}| = 325\ M\Omega$; $|Z_{para2}| = 1.2\ M\Omega$, at 1 kHz), the required probe impedances can be expected to be less than 500 kΩ at 200 Hz for ERG recordings (frequency ~500 Hz in typical ERG recordings) and less than 120 kΩ at 1 kHz for spike recordings (~10 kHz in typical spike recordings) [see Fig. D(a) in Appendix D]. However, to achieve these impedances, an Au probe tip with a diameter of more than 20 μm would be required, which would negate the low-invasiveness of the probe penetration. To reduce the probe impedance without increasing the probe-tip diameter, a material with low-impedance characteristics in saline [e.g., platinum (Pt) black or iridium oxide (IrO_x)] can be used as the tip material for the Si microprobe (Oka et al., 1999; Mailley et al., 2002).

On the other hand, we have currently developed a silicon microprobe with a tip diameter of ~50 nm (Goryu et al., 2010). The nanotip probe provides intracellular recordings with large neural amplitudes (~100 mV). Though we expect the high impedance of the nanoprobe associated with decreasing the recording area, the impedance of the nanoprobe can be reduced by utilizing aforementioned materials (Pt, IrO_x). Once neural responses are obtained via the nanoprobes, we can use the signal compensation method. The results of a small diameter high density nanoprobe array-based multi-site intracellular recording of the retina are forthcoming.

Our systematic analysis also determined that the parasitic capacitance configuration for the recording system [p–n junctions (C_{p-n}) and metal interconnections ($C_{metal/substrate}$) in the chip device and outer cables (C_{cable})] should be minimized. The parasitic impedance $|Z_{para2}|$, consisting of a parasitic resistance (R_{para}) and parasitic capacitances ($C_{para2} = C_{p-n} + C_{metal/substrate} + C_{cable}$), was 1.2 MΩ at 1 kHz, a value similar to the probe impedance (1.3 MΩ at 1 kHz). Consequently, the recorded 48% signal amplitude was mainly reduced by this parasitic impedance. Based on the parasitic impedance value, higher O/I ratios, more than 80% at 1 kHz, would be possible with reduced parasitic capacitances (C_{para2}) of less than 10% (13.1 pF) [see Fig. D(b) in Appendix D]. The reduction of these parasitic capacitances also helps to reduce crosstalk associated with adjacent interconnections. To reduce the effects of signal attenuation, phase delay, and crosstalk: (i) expanding the interconnection spacing, (ii) shortening the length of interconnections between the chip and the pre-amplifier, and (iii) integration of on-chip pre-amplifier circuitry (Sodagar et al., 2007) should be addressed in future studies.

5. Conclusion

We demonstrated multi-site ERG recordings by utilizing both an enlarged Au-tipped Si microprobe array and signal compensation of the recorded ERG responses. The enlarged Au-tipped probe enabled the reduction of the probe impedance with the increased O/I ratio in ERG recordings as compared to the Si microprobe without Au electroplating. Even though we were able to detect ERG responses via enlarged Au-tipped Si microprobes, the recorded ERG responses were attenuated and phase-delayed due to the configuration of the probe impedance and the embedded parasitic capacitances of the recording system. Thus, we used a signal compensation technique based on the investigation of the parasitic impedance system of the chip and recording system to address the attenuation and phase delay of the ERG responses. Finally, we obtained signal compensated ERG responses, which had a similar waveform to the ERG recorded by the conventional Ag–AgCl electrode. Our achievements and additional modifications of the probe chip and recording system could launch a new class of neural recording systems, with minimally invasive penetrating probes and high spatial resolution in neural recordings with the tinny probe array; this would facilitate future studies of neuronal tissues including the retina.

Acknowledgements

This work was supported in part by the Global COE Program "Frontiers of Intelligent Sensing", the Grant-in-Aid for Scientific Research (S) and the Strategic Research Program for Brain Sciences (SRPBS) from the Ministry of Education, Culture, Sports, Science and Technology (MEXT) of Japan, and the Chukyo University Research Fund.

Appendix A. Supplementary data

Supplementary data associated with this article can be found, in the online version, at doi:10.1016/j.bios.2010.10.014.

References

Asano, T., 1977. Japanese Journal of Physiology 27 (6), 701–716.
Dendo, I., 2000. Technical Report of the Institute of Electronics, Information and Communication Engineers. OME2000-150, pp. 1–7.
Greschner, M., Bongard, M., Rujan, P., Ammermüller, J., 2002. Nature Neuroscience 5, 341–347.
Goryu, A., Ikedo, A., Ishida, M., Kawano, T., 2010. Nanotechnology 21 (12), 125302.
Ishikane, H., Gangi, M., Honda, S., Tachibana, M., 2005. Nature Neuroscience 8 (8), 1087–2005.
Jones, K.E., Campbell, P.K., Normann, R.A., 1992. Annals of Biomedical Engineering 20 (4), 423–437.
Kawano, T., Takao, H., Sawada, K., Ishida, M., 2003. Japanese Journal of Applied Physics 42, 2473–2477.
Kawano, T., Kato, Y., Tani, R., Takao, H., Sawada, K., Ishida, M., 2004. IEEE Transactions on Electron Devices ED-51, 415–420.
Kawano, T., Harimoto, T., Ishihara, A., Takei, K., Kawashima, T., Usui, S., Ishida, M., 2010. Biosensors and Bioelectronics 25, 1809–1815.
Mailley, S.C., Hyland, M., Mailley, P., McLaughlin, J.M., McAdams, E.T., 2002. Materials Science and Engineering 21, 167–175.
Meister, M., Pine, J., Baylor, D.A., 1994. Journal of Neuroscience Methods 51, 95–106.
Miyake, Y., 1998. Nagoya Journal of Medical Science 61, 79–84.
Oka, H., Shimono, K., Ogawa, R., Sugihara, H., Taketani, M., 1999. Journal of Neuroscience Methods 92, 61–67.
Olveczky, B.P., Baccus, S.A., Meister, M., 2003. Nature 423, 401–408.
Penn, R.D., Hagins, W.A., 1969. Nature 223, 201–205.
Rodieck, R., 1973. The vertebrate retina: Principles of structure and function. W.H. Freeman Press, San Francisco.
Segev, R., Schneidman, E., Goodhouse, J., Berry II, M.J., 2007. Journal of Neurophysiology 98, 1380–1391.
Sieving, P.A., Murayama, K., Naarendorp, F., 1994. Neuroscience 11, 519–532.
Sodagar, A.M., Wise, K.D., Najafi, K., 2007. IEEE Transactions on Biomedical Engineering 54, 1075–1088.
Sutter, E.E., Tran, D., 1992. Vision Research 32 (3), 433–446.
Takei, K., Kawashima, T., Kawano, T., Takao, H., Sawada, K., Ishida, M., 2008. Journal of Micromechanics and Microengineering 18, 035033.
Takei, K., Kawano, T., Kawashima, T., Sawada, K., Kaneko, H., Ishida, M., 2010. Biomedical Microdevices 12, 41–48.
Wilms, M., Eckhorn, R., 2005. BMC Neuroscience 6 (50), doi:10.1186/1471-2202-6-50.